

HST Observations of IP Pegasi in Quiescence: The Pre-Eclipse Spectrum

D. W. Hoard,¹ Raymundo Baptista,² Michael Eracleous,^{3,8} Keith Horne,⁴ K. A. Misselt,⁵
Allen W. Shafter,⁶ Paula Szkody,¹ Janet H. Wood⁷

ABSTRACT

We present time-resolved HST ultraviolet spectroscopy and ground-based optical photometry of the dwarf nova IP Pegasi in a quiescent state. The observations were obtained prior to an eclipse, when the bright spot caused by the impact of the accretion stream with the edge of the disk dominates the light output. The optical light curve is fairly strongly correlated with the UV spectrophotometric flux curve. An unusual emission-like feature near 1820 Å in the UV spectrum of IP Peg is likely to be a manifestation of the “Fe II curtain.” Composite spectra constructed from the peaks and troughs of flickers in the light curve show substantial differences. The spectrum of the flickers (i.e., peaks minus troughs) is not adequately modelled by a simple blackbody, suggesting that a more sophisticated model is appropriate. We perform a cross-correlation analysis of the variability in spectrophotometric flux curves of the UV continuum and prominent UV emission lines (C II λ 1335, Si IV λ 1400, C IV λ 1550). The continuum and lines are not correlated, suggesting that they are produced separately. The C II and Si IV lines are moderately correlated with each other, but neither line is correlated with C IV, suggesting that the latter forms in a different region than the former. We briefly discuss a qualitative model for the geometry of the emission regions in IP Peg that is consistent with the observed behavior of the UV lines and continuum.

¹Department of Astronomy, University of Washington, Box 351580, Seattle, WA 98195-1580, USA

²Depto. Física, UFSC, Campus Trindade, Florianópolis, 88040-900, Brazil

³Department of Astronomy, University of California, Berkeley, CA 94720, USA

⁴School of Physics & Astronomy, University of St. Andrews, KY16 9SS St. Andrews, Fife, Scotland

⁵Department of Physics and Astronomy, Louisiana State University, Baton Rouge, LA 70803-4001, USA

⁶Department of Astronomy, San Diego State University, San Diego, CA 92182, USA

⁷Department of Physics, Keele University, Keele, Staffordshire, ST5 5BG, UK

⁸Hubble Fellow

1. Introduction

The cataclysmic variables (CVs) are semi-detached close binaries ($P_{orb} \lesssim 1$ d), in which mass is transferred from the Roche-lobe-filling, late main sequence secondary star into a rotating accretion disk around the white dwarf (WD) primary star. Mass transfer from the inner Lagrangian point at the tip of the secondary star’s Roche lobe to the outer edge of the disk occurs via an accretion stream that follows a nearly ballistic trajectory. The dwarf novae are a subclass of CV that undergo outbursts with durations of a few days to a few weeks and repeat on time scales of a few tens to a few hundreds of days. These outbursts are characterized by a rapid increase in brightness of 2–6 mag above the quiescent level. The cause of the outbursts is thought to be related to one or more instabilities in the mass transfer and/or accretion processes (see the review by Osaki 1996).

A common feature of the CV class as a whole is the presence of random, short time scale “flickering” in their light output that is thought to be produced in the accretion disk+stream. An additional (periodic) photometric modulation is often created by a bright spot that forms at the impact site of the accretion stream with the outer edge of the disk. In high inclination CVs, this bright spot is typically located directly along our line-of-sight to the system shortly before the eclipse of the hot disk+WD by the cool secondary star. The resultant increase in the level of the system’s light curve is often referred to as the “pre-eclipse hump.” The bright spot is also a probable source of flickering in CVs.

IP Peg is an eclipsing dwarf nova with orbital period 3.8 h. The eclipse is very deep ($\Delta B \approx 2.5$ mag) and the system shows a prominent pre-eclipse hump that begins near orbital phase $\phi = 0.65$ and peaks at $\phi = 0.8$ – 0.9 with $\Delta B \approx 1$ mag (Goranskij, Orlowsky, & Rahimov 1985). Marsh (1988) conducted a spectroscopic study of IP Peg in the optical regime, and calculated the following system parameters from optical emission line radial velocities: $M_{WD} = 1.09 \pm 0.10 M_{\odot}$, $M_2 = 0.64 \pm 0.09 M_{\odot}$, and $i = 79.3 \pm 0.8^{\circ}$. Marsh also isolated the spectrum of the bright spot by subtracting the average spectrum during phases outside both the pre-eclipse hump and the eclipse from a spectrum obtained at the peak of the hump. A blackbody with temperature $T = 12,000 \pm 1000$ K produces the best fit to the continuum of the bright spot spectrum. Szkody (1987), on the other hand, used a similar method applied to an *International Ultraviolet Explorer* (IUE) spectrum of IP Peg to determine a blackbody temperature of $T \approx 20,000$ K for the bright spot. Doppler tomography of IP Peg in the Balmer lines shows a fairly uniform disk structure with a bright spot at the expected site of the accretion stream impact; the brightness of the spot varies in tomograms constructed from spectra obtained several years apart (Marsh & Horne 1990, Kaitchuck et al. 1994). This apparent variability of the bright spot radiation may explain the different temperatures determined by Szkody and Marsh, or it may be due

to observing a temperature-stratified spot in different wavelength regimes – the dwarf nova Z Chamaeleontis showed a similar discrepancy between bright spot temperatures determined from optical ($T \approx 11,300$ K; Wood et al. 1986) and UV ($T \approx 16,700$ K; Robinson et al. 1995) observations.

IP Peg was observed with the Faint Object Spectrograph (FOS) on the *Hubble Space Telescope* (HST) on 9 occasions between 1992 November and 1994 October. The first 7 observations are presented in Baptista et al. (1994), while a paper presenting the entire set of observations in detail is in preparation. Here we concentrate on the first observation, which was carried out on 1992 November 2 UT. The goal of this observation was to obtain time-resolved spectrophotometry during eclipse while the system was in a quiescent state. Due to a scheduling error, however, Run 1 was obtained during ingress to eclipse rather than during the eclipse itself. These pre-eclipse measurements can be utilized to study the rapid timescale flickering associated with the bright spot and beginning of eclipse in IP Peg. We report here on the results of our analysis of the Run 1 observations and simultaneous ground-based photometry of IP Peg.

2. Observations

2.1. HST Ultraviolet Spectra

The observation started at UT 08:17 (HJD 2448928.84955) and spanned a single spacecraft orbit. During the part of the orbit when the target was visible to the telescope (40 minutes), 437 spectra were taken in rapid succession, with an exposure time of 1.18 s and a time resolution of 5.5 s. The spectra were obtained through a $4''.3$ aperture, using the G160L grating, which gave a spectral resolution of 9.2 \AA (FWHM) over the range $1150 - 2500 \text{ \AA}$. The blue ends of the spectra are severely contaminated by geocoronal Ly α emission, while the 2nd order geocoronal Ly α emission contaminates the red ends at the few percent level. Using the IP Peg eclipse ephemeris of Wolf et al. (1993)

$$HJD_{min} = 2445615.4224(4) + 0.15820616(4)E, \quad (1)$$

the observations cover the orbital phase range $\phi \approx 0.73-0.91$.

The data reduction consisted of background subtraction, flat field division, and flux calibration. The background subtraction involved the scaling of the nominal background spectrum to the observed time-dependent background level, as recorded by the “unilluminated” segments of the detector array. Thus, this method corrects not only for the particle background but also for contamination by light scattered within the spectrograph. The ge-

omagnetic image motion problem (GIMP) amounted to wavelength-scale shifts of less than 0.5 pixels (0.9 Å) for 80% of the spectra, and was not corrected.

2.2. HST Broad-band Photometry

In addition to the 1st order dispersed light, the 0th order undispersed light was also recorded by the detector array, and provided a broad-band optical/UV count rate for IP Peg. The passband of the 0th order light has a pivot wavelength of 3400 Å, a full-width at half-peak response of 1900 Å, and an effective response of 520 counts s⁻¹ mJy⁻¹ (accurate to 50% – Horne & Eracleous 1993; Eracleous et al. 1994). The 0th order count rates were converted to an arbitrary magnitude scale via the relation

$$mag = 12.0 - 2.5 \log(count\ rate) = 9.28 - 2.5 \log \left[\frac{f_\nu(3400\text{\AA})}{1\text{ mJy}} \right] \quad (2)$$

in order to facilitate comparison with ground-based photometry of IP Peg. As with the spectra, the photometric measurements have a time resolution of 5.5 s.

2.3. Ground-based Optical Photometry

Simultaneous ground-based photometry of IP Peg was obtained with a TI 800 × 800 pixel CCD on the 1-m telescope at the Mount Laguna Observatory. Several sub-fields on the CCD were read out into a contiguous image to provide a number of comparison stars while minimizing image size and dead time – for a more complete description of the Mount Laguna CCD, see Shafter, Misselt, & Veal (1993). Measurements were made through a *V* filter, with a time resolution of approximately 30 s, between HJD = 2448928.77492 and HJD = 2448928.88362. The images were processed in the usual fashion (i.e., bias-subtracted and flat-field-corrected) using standard IRAF¹ routines. The reduced stellar count rates were converted to magnitudes via aperture photometry. The magnitude of a comparison star was subtracted from that of IP Peg to remove the effects of atmospheric extinction and sky transparency variations. The ground-based data overlaps all of the HST Run 1 observations.

¹i.e., the Image Reduction and Analysis Facility operated by the National Optical Astronomy Observatories

3. Results

3.1. The Light Curve of IP Peg during Run 1

The HST light curve of IP Peg obtained from the 0th order passband of the FOS observations is shown in the top panel of Figure 1. Rapid oscillations with amplitude ≈ 0.3 mag on timescales of ≈ 0.002 days (about 3 minutes) are visible. The middle panel of Figure 1 shows the simultaneous ground-based light curve of IP Peg. The light curves decline rapidly by ≈ 1 mag over 0.003 d as the system enters eclipse after HJD = 2448928.872. For a first, qualitative comparison of the two data sets, the HST data was binned to the same time resolution of the ground-based data (bottom panel of Figure 1). The two light curves show similarities, the most conspicuous one being the prominent peak near HJD 2448928.853. Unfortunately, this agreement is achieved at the expense of smearing out the short timescale variability seen in the higher time resolution, unbinned HST light curve.

In order to gauge the similarity of the two light curves in a quantitative manner, *Interactive Data Language* (IDL) routines were used to calculate the Fourier cross-correlation function of the two data sets. First, the overlapping segments of the light curves from HJD = 2448928.85 until the steep ingress to the eclipse at HJD = 2448928.875 were re-binned into equally-spaced time series containing 100 points each. Next, a second order spline function was subtracted from each light curve to remove long time scale variations. Finally, the cross-correlation was performed and yielded a peak amplitude of $\approx +0.54$. A perfect correlation (e.g., from comparing identical data sets) would yield an amplitude of 1.0, so this result indicates a reasonably strong positive correlation between the variability in the two light curves. A negative amplitude would have indicated an anti-correlation; that is, one of the light curves would show a maximum at the same time the other showed a minimum. In addition, the peak of the cross-correlation function occurs in bin 0, which indicates that there is no time lag between the variability in the two light curves that is larger than the time resolution of the binned data (~ 30 s). Another measure of the strength of the correlation is obtained from the R parameter (Tonry & Davis 1979), which is the ratio of the amplitude of a given peak to the average amplitude of peaks in the cross-correlation function,

$$R = \frac{h}{\sqrt{2}\sigma_a}, \quad (3)$$

where h = the peak height, σ_a = the noise level of the cross-correlation function, and $\sqrt{2}\sigma_a$ = the average peak height in the cross-correlation function. The larger the value of R , the more significant is the correlation; for example, a nearly perfect correlation ($h = 0.9$) in the presence of noise at the 10% level ($\sigma_a = 0.1$) in the cross-correlation function would yield $R \approx 6.4$, while a correlation peak with an amplitude of only twice the noise level would

yield $R \approx 1.4$. For the IP Peg light curve cross-correlation, we obtain a correlation peak with $R \approx 3.6$, corresponding to a peak with amplitude of about 5 times the noise level in the cross-correlation function.

Although the behavior of the HST 0th order and ground-based V light curves of IP Peg is fairly strongly correlated – which indicates that the source of the short timescale variability radiates over a wavelength range of $\approx 3400\text{--}5500 \text{ \AA}$ – it should be kept in mind that, as mentioned above, the shortest timescale oscillations cannot be detected in the lower time

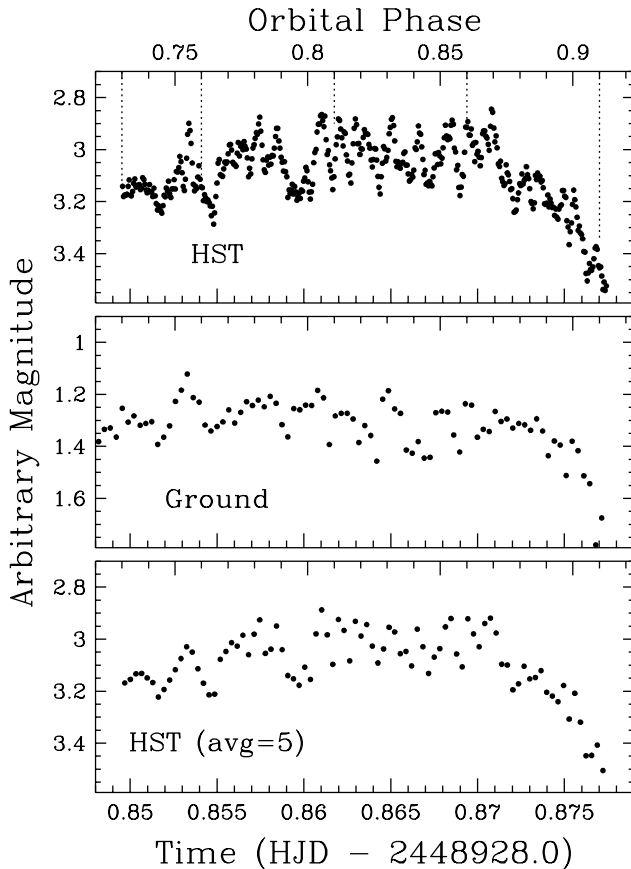


Fig. 1.— The ground-based (middle panel) and 0th order HST light curves of IP Peg on 1992 November 2 UT. The top panel shows the full 5.5 s resolution of the HST data while the bottom panel has been averaged over five points to simulate the time resolution of the ground-based data. The horizontal axis at the top of each panel is calibrated in orbital phase according to the ephemeris of Wolf et al. (1993); the horizontal axis at the bottom of each panel is calibrated in HJD. The dotted lines in the top panel mark the limits used to construct the phase-resolved spectra described in §3.2.2 and shown in Figure 4.

resolution ground-based data. Thus, there may yet be wavelength dependent differences between the 0th order and V filter bandpasses at the very short timescales of the flickering seen in the unbinned HST light curve.

We also calculated the cross-correlation of the 0th order undispersed light curve and a spectrophotometric “flux curve” of the UV continuum ($\lambda \approx 2000\text{--}2100 \text{ \AA}$) from the 1st order dispersed light (see §3.2.4). However, no significant correlation was found (the highest peak in the cross-correlation function has amplitude $\lesssim 0.15$ and is comparable to the typical amplitude of random peaks). This implies that the source of the continuum radiation in IP Peg is different in the UV than in the optical.

3.2. The Ultraviolet Spectrum of IP Peg during Run 1

The average HST spectrum of IP Peg is shown in Figure 2. The spectrum displays a number of emission lines of various elements, primarily carbon (C II $\lambda 1335$, C IV $\lambda 1550$) and silicon (Si IV $\lambda 1400$). There is also an unusual and unidentified emission-like feature centered around $\lambda \approx 1820 \text{ \AA}$.

3.2.1. The 1820 \AA Feature

This feature in the ultraviolet spectrum is plateau-like. It peaks at $\approx 1820 \text{ \AA}$, showing a width of $\approx 75 \text{ \AA}$ and an intensity of about $2 \times 10^{-15} \text{ ergs s}^{-1} \text{ cm}^{-2} \text{ \AA}^{-1}$ above the local continuum level, comparable to that of the carbon and silicon lines. Its long wavelength edge is very sharp. The IUE spectrum of IP Peg obtained by Szkody (1987) over similar wavelength range, orbital phase, and total exposure time does *not* display this feature. It is weakly present in spectra obtained with an identical FOS configuration during the eclipse of IP Peg in Run 3 of our 1992 November HST observations and is very strong in follow-up HST observations of IP Peg obtained during decline from an outburst in 1993 May; however, it is completely gone in HST/FOS spectra taken during an outburst (Baptista et al. 1994). We have examined the possible origin of this feature as (a) a data artifact, (b) a superposition of emission lines, or (c) a gap between broad absorption bands.

(a) Incorrect flat-fielding of FOS images can produce erroneous features in the spectra with characteristics similar to those of the 1820 \AA feature (Leitherer 1995). In addition, the G160L disperser is subject to large ($> 5\%$) inaccuracies in the time-dependent behavior of its flat-field. An inspection of the flat-field in that spectral region, however, did not reveal any irregularities. Figure 3 shows the average spectrum of IP Peg from Runs 1, 2, and 9.

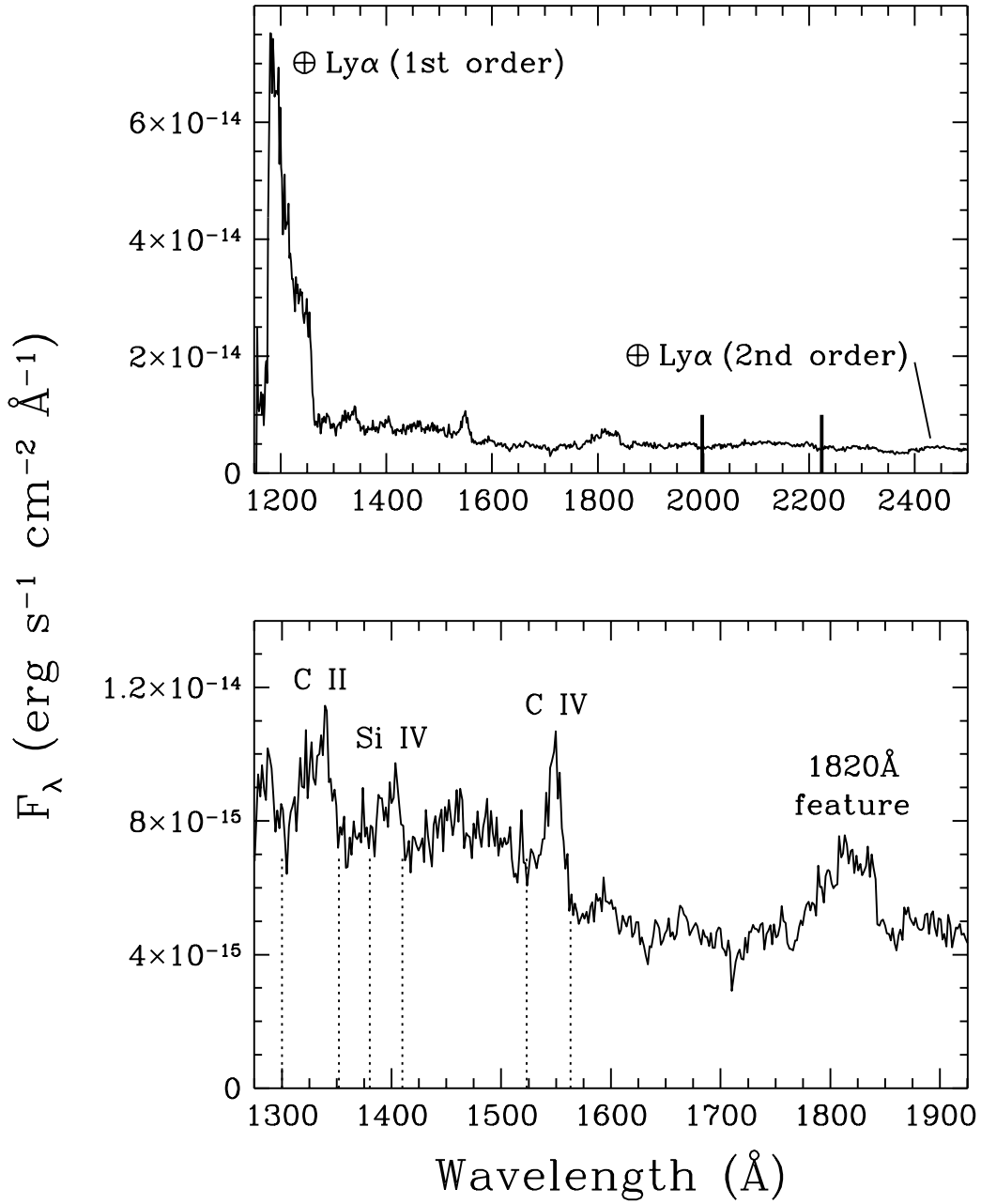


Fig. 2.— The average HST/FOS spectrum of IP Peg from Run 1 on 1992 November 2 UT. The top panel shows the entire spectrum with the positions of the first- and second-order (geocoronal) Ly α emission indicated. The dark vertical bars near 2000 \AA and 2200 \AA mark the limits of the region from which the continuum flux curves used in the cross-correlation analysis were obtained. The bottom panel is an enlargement of the central region of the spectrum showing the emission lines of carbon (C II λ 1335, C IV λ 1550) and silicon (Si IV λ 1400), as well as the unusual feature at $\lambda \approx 1820$ \AA . The dotted lines mark the limits of the wavelength regions from which the emission line flux curves used in the cross-correlation analysis were obtained.

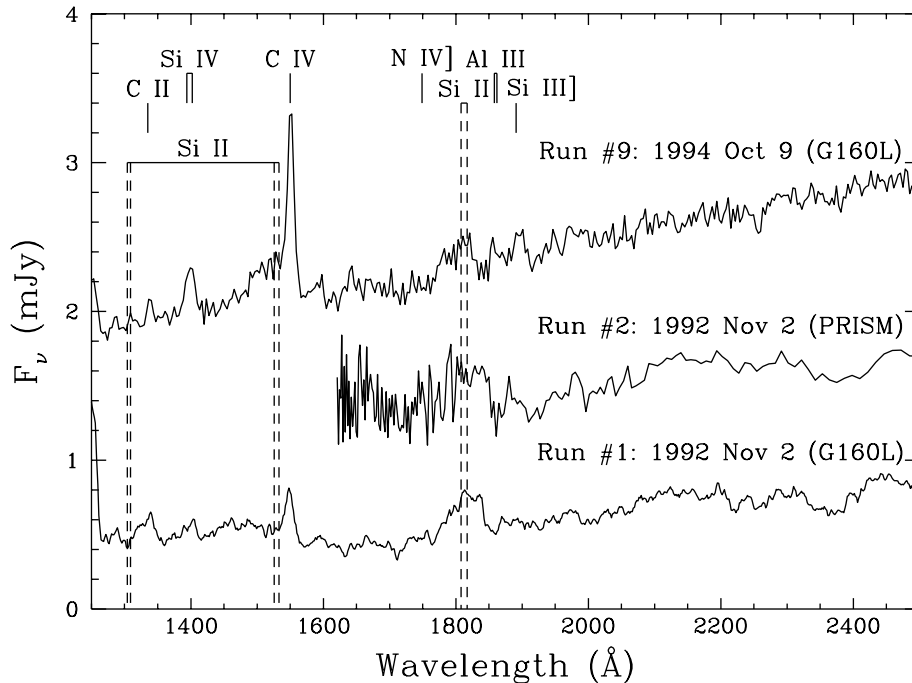


Fig. 3.— HST/FOS spectra of IP Peg obtained on the same day using different optical elements (Runs 1 and 2), and on a different day two years later (following the decline from an outburst) using the same optical elements as in Run 1 (Run 9). The flux scale refers to the bottom spectrum (Run 1) and the remaining spectra have been separated by 0.75 mJy. The positions of several spectral lines are indicated.

The last two of these were HST/FOS observing runs similar in nature to Run 1 as it is described in §2.1. The spectra in Run 2 (Baptista et al. 1994) were obtained on the same day as Run 1, but using the PRISM rather than the G160L grating. Run 9 (which will be described in detail in a future paper) was obtained with the same grating as Run 1, but ≈ 2 yr later following the decline from an outburst of IP Peg. The 1820 Å feature is visible in all three of these spectra. The fact that it appears in both the PRISM and G160L spectra rules out an instrumental artifact because in these two configurations the spectra fall on different locations on the FOS/BLUE photocathode and are recorded by different parts of the diode array.

(b) Although Si II has lines at 1808 Å and 1817 Å, the width and oddly-shaped profile of the 1820 Å feature is not expected from simple line emission. If the Si II doublet were contributing a large amount of the flux, then we might expect the profile of the 1820 Å feature to look more like the strong (unresolved) doublet of Si IV near 1400 Å. In addition, Si II has two other doublet-producing transitions to the ground state (at 1304, 1309 Å and 1526, 1533 Å) that we would expect to see if the 1808, 1817 Å doublet was strong. These

additional doublets are not visible in the spectra of IP Peg (see Fig. 3).

(c) A feature similar to the one at $\approx 1820 \text{ \AA}$ in the spectrum of IP Peg is observed in the spectrum of the cataclysmic variable OY Car. In the case of OY Car, the feature is thought to be a region of continuum that appears to be in emission because it is sandwiched between two adjacent absorption bands of the “Fe II curtain” discussed by Horne et al. (1994). Yet, there are a number of differences between the spectra of IP Peg and OY Car. For example, while there is some indication of the presence of an absorption band on the short wavelength side of the 1820 \AA feature in IP Peg, the long wavelength side is relatively smooth and constant as far out as the beginning of the 2nd order geocoronal Ly α emission. The latter region, at least, is quite continuum-like, with no apparent absorption bands. There does seem to be a rather abrupt drop in the (apparent) continuum level from the short-wavelength side of the C IV $\lambda 1550$ line to the long-wavelength side, and the flux level of the 1820 \AA feature is very close to that of the continuum level shortward of C IV. This suggests the possibility that the flux level across the entire spectral region from $\approx 1550 \text{ \AA}$ to $\approx 1750 \text{ \AA}$ may be suppressed by absorption bands of the Fe II curtain. The fact that the spectrum of IP Peg does not resemble the spectrum of OY Car very closely does not necessarily preclude the presence of an Fe curtain of some sort. It is possible that the ionization structure of the curtain is different in the two stars (e.g., due to a difference in the luminosity of the background source or a change in the column density caused by a difference in inclination angle). The absence of the 1820 \AA feature in the IUE spectrum presented by Szkody (1987) may also be related to changes in the ionization structure of the absorbing curtain.

Although the actual origin of the 1820 \AA feature in the spectrum of IP Peg is not yet certain, we believe that data artifacts and contribution from underlying emission lines can be ruled out. Despite the cosmetic differences between the spectrum of IP Peg and OY Car, this leaves a manifestation of the Fe II curtain as the most likely cause for the 1820 \AA feature.

3.2.2. *The Emission Lines*

The fluxes and equivalent widths of the prominent emission lines in the average HST spectrum of IP Peg were measured by direct integration of the pixel intensities between two manually-selected endpoints. The results are shown in Table 1. In each case, the line parameters were measured from the spectrum three separate times; the tabulated results are the average values and standard deviation of these three trials. The uncertainties in the averages of the measured line centers are all much smaller than 1 \AA . Also listed in Table 1 are the flux and equivalent width of the C IV $\lambda 1550$ line from the IUE spectrum of IP Peg obtained over a similar range of orbital phase as the HST spectrum, but six years earlier,

TABLE 1
ULTRAVIOLET LINE FLUXES AND EQUIVALENT WIDTHS FOR IP PEG

Line	Measured Center (Å)	Continuum Level (10 ⁻¹⁵ ergs/s/cm ² /Å)	Line Flux (10 ⁻¹⁵ ergs/s/cm ²)	Equivalent Width (Å)
<u>HST ($\phi = 0.73-0.91$):</u>				
C II $\lambda 1335$	1333	7.6(1)	72.6(1)	9.5(1)
Si IV $\lambda 1400$	1399	7.2(1)	33.8(4)	4.7(1)
C IV $\lambda 1550$	1548	6.3(2)	56.0(7)	8.9(2)
<u>IUE ($\phi = 0.72-0.94$):</u>				
C IV $\lambda 1550$	150	15

on 1986 August 22 UT (= JD 2446664; Szkody 1987). The flux of the C IV line in the IUE spectrum is almost three times that in the HST spectrum, and the equivalent width is about twice as large in the former. IP Peg was in a quiescent state during both of these observations: the *Variable Star Network* (<http://www.kusastro.kyoto-u.ac.jp/vsnet/>) long-term light curve for IP Peg shows it to have been between outbursts, with $V \approx 15-16$. Also, the continuum levels in the IUE and HST spectra are comparable, at $F_\lambda \approx 0.5-1.0 \times 10^{-14}$ erg s⁻¹ cm⁻² Å⁻¹. Because of the large time difference between the two spectra, however, it is not clear whether these differences reflect the range of orbit-to-orbit variability of the emission lines or an actual long term change in the emission characteristics of IP Peg.

Since changes in the nature of its spectrum should be expected as IP Peg goes into eclipse, the averaged spectrum was divided into several successive sub-spectra: one of width 0.03 (starting at $\phi = 0.73$) and three covering phase bins of width 0.05 (ending at $\phi = 0.91$). These phase-resolved spectra of IP Peg are shown in Figure 4. The line fluxes and equivalent widths in the earliest (out of eclipse) and the latest (beginning of eclipse) of the spectra with phase bin widths of $\Delta\phi = 0.05$ were measured as described above; the results are shown in Table 2. With the exception of the Si IV line, which shows an essentially unchanged equivalent width from one spectrum to the other, the widths of the carbon lines are lower in the out of eclipse spectrum by a factor of $\approx 2-4$. In both of the carbon lines, the flux level at the beginning of eclipse is larger than that at out of eclipse phases. The Si IV line, on the other hand, has a larger flux outside of eclipse. This suggests that the Si IV line may be originating in a narrower, more central region in the disk than the carbon lines; hence, the former is being eclipsed more than the latter.

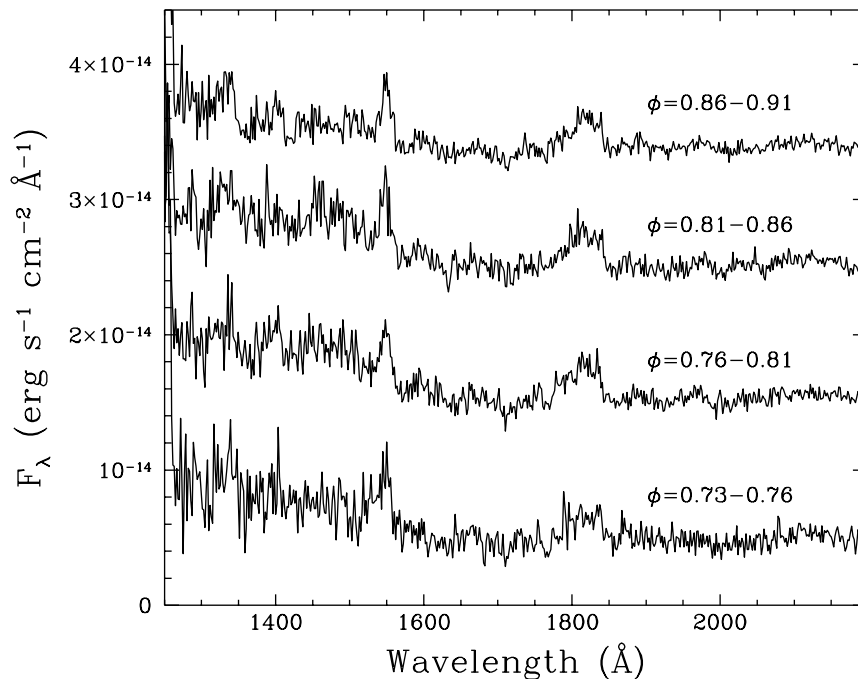


Fig. 4.— The phase-resolved spectra of IP Peg. The flux scale refers to the bottom spectrum and $1.0 \times 10^{-14} \text{ erg s}^{-1} \text{ cm}^{-2} \text{ \AA}^{-1}$ has been cumulatively added to each spectrum above it.

3.2.3. The Flickering Spectrum

We determined the mean flux level of each HST spectrum in the wavelength interval 1300–2200 \AA , then calculated the average and standard deviation (σ_{mean}) of the mean flux levels. All of the spectra with mean flux levels greater than $1\sigma_{mean}$ above the average were combined to give the spectrum of IP Peg at the peaks of the UV flickering (henceforth, the high spectrum), while those with mean levels less than $1\sigma_{mean}$ below the average were combined to give the spectrum between flickers (henceforth, the low spectrum). The low spectrum was then subtracted from the high spectrum to obtain the wavelength-dependence of the UV flickering amplitude (henceforth, the flickering spectrum). These three spectra are shown in Figure 5.

The C IV line is present with comparable strength in both the high and low spectra. The C II and Si IV lines, on the other hand, are only apparent in the high spectrum. This suggests a possible relationship between the C II and Si IV emission sources that is not shared by the source of the C IV emission.

TABLE 2
PHASE-RESOLVED LINE FLUXES AND EQUIVALENT WIDTHS

Line	Measured Center (Å)	Continuum Level (10 ⁻¹⁵ ergs/s/cm ² /Å)	Line Flux (10 ⁻¹⁵ ergs/s/cm ²)	Equivalent Width (Å)
Out of Eclipse ($\phi = 0.76-0.81$):				
C II $\lambda 1335$	1338	8.6(1)	36.7(5)	4.3(1)
Si IV $\lambda 1400$	1397	8.1(1)	58.5(1.1)	7.2(2)
C IV $\lambda 1550$	1548	6.9(1)	52.0(6)	7.6(2)
Beginning of Eclipse: ($\phi = 0.86-0.91$):				
C II $\lambda 1335$	1332	4.9(1)	90.0(4.0)	18.3(8)
Si IV $\lambda 1400$	1402	4.7(1)	34.9(1.5)	7.4(3)
C IV $\lambda 1550$	1548	4.2(1)	71.0(6)	16.9(1)

The 1820 Å feature is visible in both the high and low spectra, but is almost entirely gone in the flickering spectrum. The high and low spectra were constructed from approximately equal-number samples of more-or-less randomly distributed spectra in the original continuous series of spectra. Thus, a feature which is equally visible in all of the original spectra (e.g., due to the effect of an Fe II curtain) should be present with equal strength in both the high and low spectra. This would cause it to be totally subtracted in the flickering spectrum, as is observed for the 1820 Å feature.

There is a region of excess flux in the flickering spectrum between ≈ 1300 Å and ≈ 1500 Å, which indicates that a large fraction of the UV flickering originates in this wavelength region. An obvious conclusion is that this excess flux represents the contribution of the bright spot. A blackbody with $T \approx 22,000$ K would peak near the center of this feature, at $\lambda \approx 1400$ Å. This temperature is comparable to that determined for the bright spot in IP Peg from IUE observations (Szkody 1987); however, attempts to fit a blackbody curve to the HST flickering spectrum were unsuccessful because of the narrowness of the excess flux feature and the sharp drop in flux shortward of ≈ 1300 Å. The dashed line in the bottom panel of Figure 5 shows an arbitrarily-scaled blackbody curve for $T = 22,000$ K. Although the slope of the curve longward of ≈ 1500 Å is a reasonable match to the data, the shape of the curve deviates significantly from the data at shorter wavelengths. The flickering spectrum does not appear to be adequately modelled by a simple blackbody, suggesting that a more sophisticated model is appropriate. For example, a disk atmosphere spectrum might account for the depression shortward of 1300 Å as a broad Ly α absorption line. For now, however, the origin of the excess flux and short-wavelength flux drop-off in the wavelength-dependence of the UV flickering amplitude are unclear.

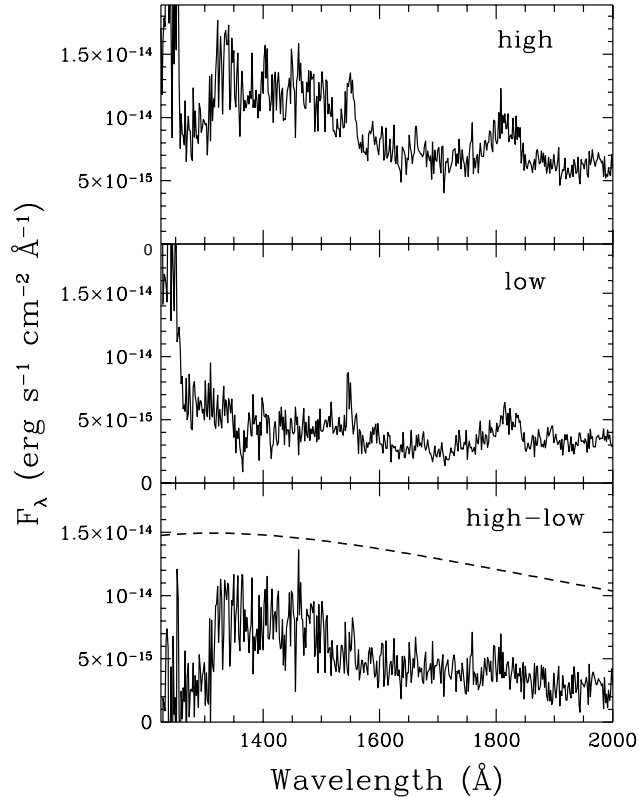


Fig. 5.— The top panel shows the average “high” spectrum of IP Peg obtained at the peaks of the flickering. The middle panel shows the average “low” spectrum obtained between flickers. The bottom panel is the difference of the high and low spectra, showing the wavelength-dependence of the flickering amplitude. The dashed line in the bottom panel is an arbitrarily-scaled blackbody curve with $T = 22,000$ K for comparison.

3.2.4. Comparison of Line and Continuum Flickering

Spectrophotometric “flux curves” were constructed from the IP Peg spectra by averaging (with equal weights) the pixel values in a specific wavelength range (spectral bin) in each spectrum. Because the wavelength scale is linear to a high degree of accuracy, this average with equal weights is valid even for a reasonably wide spectral bin and for bins taken from different regions of the spectra. The pixel and wavelength ranges used, along with the mean values of the resultant flux curves, are listed in Table 3. The primary wavelength regions were centered around the C II, Si IV, and C IV emission lines, as well as around two regions of pure continuum. We also created flux curves from small continuum regions located adjacent to both endpoints of the emission line spectral bins.

TABLE 3
SPECTROPHOTOMETRIC FLUX CURVES

Name	Pixel Range	# of pixels	Wavelength Range (Å)	Mean Flux (10^{-15} ergs s $^{-1}$ cm $^{-2}$ Å $^{-1}$ pixel $^{-1}$)
continuum A-1	213–231	19	1270–1299	9.1(4.8)
C II+continuum	232–262	31	1300–1352	9.3(3.8)
continuum A-2	263–277	15	1354–1379	7.7(4.3)
continuum B-1	263–277	15	1354–1379	7.7(4.3)
Si IV+continuum	278–294	17	1380–1410	8.5(4.0)
continuum B-2	295–311	17	1410–1438	7.4(3.8)
continuum C-1	336–359	24	1481–1521	7.6(3.2)
C IV+continuum	360–383	24	1523–1563	7.7(2.6)
continuum C-2	384–407	24	1565–1605	5.5(2.1)
continuum 1	633–704	72	1998–2121	4.9(1.2)
continuum 2	692–763	72	2100–2224	4.9(1.3)

The wavelength ranges of the small continuum regions adjacent to the lines were chosen to minimize contamination from other spectral lines. In general, these continuum regions are line-free, with the exception that O V λ 1371 falls in A-2/B-1 and N IV] λ 1487 falls in C-1. However, we inspected the average spectrum of IP Peg and found no evidence for the presence of these lines above the scatter in the continuum level. In order to isolate the flickering behavior of the emission lines from that of the underlying continuum, the pair of continuum flux curves for the regions adjacent to each line were averaged together and subtracted from the flux curves of the corresponding line regions. The mean values and 1σ standard deviations of the averaged continuum flux curves and the continuum-subtracted line flux curves are shown in Table 4.

The IP Peg flux curves were cross-correlated as in §3.1 according to the pairings listed in Table 5. The first few cases test the continuum region flux curves for contamination from non-continuum flickering, in order to ensure that the regions used are truly representative of the continuum behavior.

Case 1: These two continuum sections were chosen from a line-free region of the spectrum. Their high degree of correlation implies that there is little or no contamination from flux variability other than random noise differences between the two continuum regions; that is, these regions appear to be pure continuum.

TABLE 4
AVERAGE FLUX CURVE VALUES

Name	Mean Flux (10^{-15} ergs s $^{-1}$ cm $^{-2}$ Å $^{-1}$ pixel $^{-1}$)
continuum A	8.4(3.5)
continuum B	7.6(3.4)
continuum C	6.5(2.4)
C II line only	0.8(3.8)
Si IV line only	0.9(3.6)
C IV line only	1.2(2.5)

Cases 2, 3, 4: These cases compare one of the pure continuum samples with the flux curves of the continuum regions adjacent to the lines, which were subtracted from the line flux curves to remove the continuum contribution. The average continuum flux curves used to background-subtract the emission lines are highly correlated with the pure continuum.

The next six cases provide additional tests of the cross-correlation procedure by comparing flux curves whose cross-correlation has a predictable outcome.

Cases 5, 6, 7: These cases are highly correlated, as expected due to the presence of the line flickering component in both the line-only and line-plus-continuum flux curves.

Cases 8, 9, 10: These cases are also highly correlated, as expected due to the presence of the continuum flickering component in both the line-plus-continuum and continuum-only flux curves.

Finally, the remaining cases deal with the actual comparisons of interest here, from line-to-line and line-to-continuum.

Cases 11, 12, 13: These cases are expected to show a high degree of correlation if the different emission lines are varying in the same fashion. This would imply that the lines originate from the same region in the system. The fact that the C II and Si IV lines *are* correlated with each other (Case 11), while neither is correlated with the C IV line (Cases 12 and 13), suggests two possible conclusions: (a) the C II and Si IV lines actually are correlated with the C IV line, but at a level that is small compared to the noise in the flux curves, or (b) the C II and Si IV lines originate in the same physical region of the system and it is a different region than that in which the C IV

TABLE 5
FLUX CURVE CROSS-CORRELATION RESULTS

Case	Cross-Correlation	Correlation Peak Parameters:			
		Center ^a	Amplitude	R Value	Confidence ^b
1	continuum 1 to continuum 2	0	0.80	10.9	1.00
2	continuum A to continuum 1	0	0.47	9.7	1.00
3	continuum B to continuum 1	0	0.64	9.2	1.00
4	continuum C to continuum 1	0	0.65	10.3	1.00
5	C II line to C II+continuum	0	0.62	14.2	1.00
6	Si IV line to Si IV+continuum	0	0.65	12.6	1.00
7	C IV line to C IV+continuum	0	0.63	13.0	1.00
8	C II+continuum to continuum 1	0	0.43	10.2	1.00
9	Si IV+continuum to continuum 1	0	0.47	8.5	1.00
10	C IV+continuum to continuum 1	0	0.48	8.6	1.00
11	Si IV line to C II line	0	0.19	4.6	1.00
12	Si IV line to C IV line	(-54) ^c	(0.14)	(3.1)	(0.83)
13	C II line to C IV line	(-96)	(0.12)	(2.5)	(0.28)
14	C II line to continuum 1	(-46)	(0.12)	(2.9)	(0.70)
15	Si IV line to continuum 1	(-80)	(0.14)	(3.2)	(0.88)
16	C IV line to continuum 1	(77)	(0.14)	(3.2)	(0.86)

^aIf the peak in the cross-correlation function is centered at 0, then there is no time delay between the data sets. Non-zero offsets are measured in bins with size equal to the spacing of the data; i.e., 5.5 s bin^{-1} for the HST spectra of IP Peg.

^bFollowing Tonry & Davis (1979), the confidence level of the peak in the cross-correlation function; i.e., the probability that the chosen peak corresponds to the maximum in the cross-correlation function.

^cValues in parentheses are representative upper limit values for the highest peaks in cross-correlation functions containing no obvious dominant peak.

line originates. We favor the second possibility, which is also supported by the relative strengths of the emission lines in the high and low flickering spectra of IP Peg (see §3.2.3), as well as the fact that the relatively high ionization energy of C IV ($\chi = 64.5$ eV) suggests that this line is likely to originate in a more energetic region than either Si IV ($\chi = 45.1$ eV) or C II ($\chi = 24.4$ eV).

Cases 14, 15, 16: These cases are expected to show a high degree of correlation only if the lines and continuum are varying together. Since none of the cases shows significant correlation, it must be true that the lines and continuum behave independently of each other.

The amplitudes and R values of the peak in Case 11 are not much larger than those of the peaks in the remaining higher-numbered cases. Hence, one might ask why the former peak is considered significant, while the latter are not? The rightmost column in Table 5 lists a confidence level (which was calculated as in Tonry & Davis 1979) corresponding to the selected peak in the cross-correlation function. Through Case 11, this confidence level is 1.00, indicating that the chosen peak is the true maximum in the cross-correlation function. While it is not difficult to accept that the peak in Case 13, with a confidence level of only 0.28, is spurious, the remaining cases beyond Case 11 have confidence levels of ≈ 0.7 – 0.9 . We might normally be inclined to accept a result of which we are 80% confident; however, a “normal” interpretation of the confidence level is not applicable in this case. The error function for the cross-correlation peak changes rapidly for small values of R then levels out at larger values of R (e.g., see Fig. 14 in Tonry & Davis 1979). Consequently, while a confidence level of 1.00 does indicate that the correlation is highly significant, a spurious peak in the cross-correlation function can produce a confidence level only a few percent smaller. This is best illustrated by comparing plots of the cross-correlation functions for several cases that have different peak amplitudes, R values, and confidence levels. Figure 6 shows the cross-correlation functions of Cases 5, 11, 12, and 13. The strong peak in Case 5 has a high amplitude, large R value, and confidence level of 1.00 (see Table 5). The height of the peak in Case 11 (which also has a confidence level of 1.00) is still well in excess of the noise fluctuations in the rest of the curve, despite its relatively smaller amplitude and R value. The remaining two plots, on the other hand, do not contain an obvious dominant peak. The cross-correlation function of Case 12, whose highest peak has a confidence level of ≈ 0.8 , does not contain any single peak that is preferable over others and is visually indistinguishable from Case 13, whose highest peak has only a low confidence level (≈ 0.3).

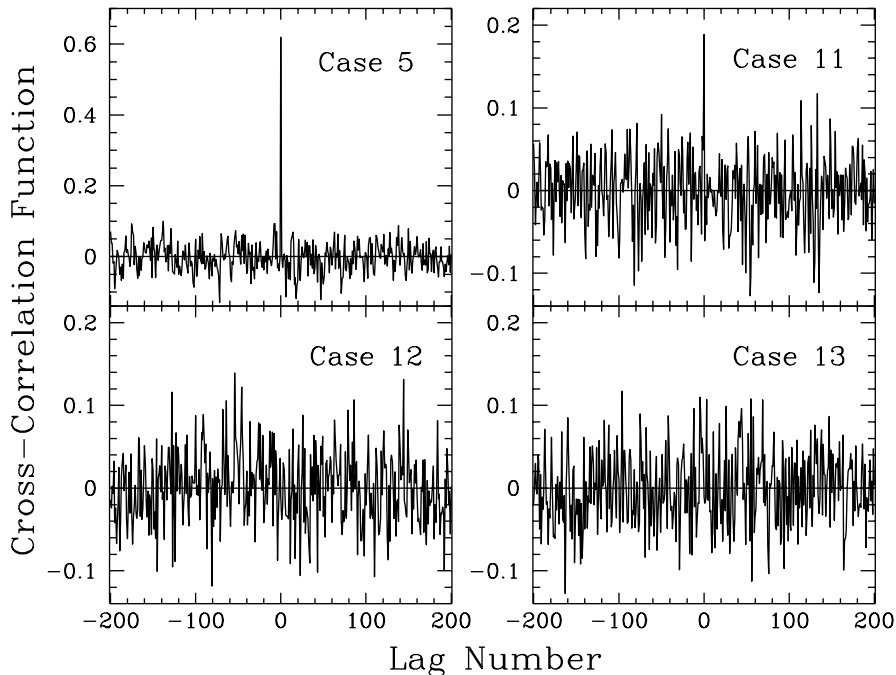


Fig. 6.— The cross-correlation functions for Cases 5, 11, 12, and 13 (see Table 5). Only Cases 5 and 11 exhibit a significant correlation.

4. Discussion and Conclusions

The flickering in the simultaneous ground-based optical (V -band) and HST broad-band (undispersed 0th order) light curves of IP Peg shows a fairly strong degree of correlation. This suggests that the source of the optical continuum radiation emits over a wavelength interval of at least $\approx 3400\text{--}5500 \text{ \AA}$; however, the difference in time resolution between the two data sets (i.e., the low time resolution of the ground-based data) prevents a more detailed comparison of the flickering at these wavelengths. On the other hand, the optical continuum is not correlated with the UV continuum, which implies that the continuum radiation has a different source shortward of $\lambda \sim 2200 \text{ \AA}$. None of the UV emission line flickering shows a significant degree of correlation with that of the UV continuum, which indicates that the lines and continuum are produced by separate mechanisms and/or in different locations in the IP Peg system.

In both of the emission lines of carbon (C II and C IV), the line fluxes at the beginning of eclipse ($\phi = 0.86\text{--}0.91$) are larger than those out of eclipse ($\phi = 0.76\text{--}0.81$). The Si IV line, on the other hand, has a larger flux outside of eclipse. Also, the equivalent widths of the carbon lines increase by factors of $\approx 2\text{--}4$ between the out of eclipse and beginning of eclipse

spectra, but the equivalent width of the silicon line remains approximately constant. This suggests that the Si IV emission may be originating in a narrower, more central region in the disk than the carbon lines; hence, the former is being eclipsed more than the latter. An equivalent statement is that there may be carbon, but not silicon, emission that is visible as the system goes into eclipse, possibly originating in a vertically-extended corona/wind from the disk.

While the C II and Si IV emission line flickering is moderately correlated, neither is correlated with the flickering of the C IV line. This suggests that the C IV line originates from a different physical location in the IP Peg system than the other two lines. This conclusion is also supported by a comparison of the relative strengths of the emission lines in the high and low flickering spectra of IP Peg. Yet, it appears to contradict somewhat the flux level and equivalent width behavior of the emission lines going into eclipse, which shows that the two carbon lines behave similarly to each other and differently from the silicon line. This dilemma could be resolved if, for example, the vertical structure above and below the accretion disk is stratified into a hot corona with an equilibrium configuration close to the disk surface, and an outflowing wind that dominates further away from the disk. A similar model was discussed by Meyer & Meyer-Hofmeister (1994) as it relates to the dissipation of the inner disk in dwarf novae via a coronal siphon flow. If the Si IV emission originates in the corona near the disk surface, the C II originates in the upper corona, and the C IV emission originates in the wind, then both carbon emitting regions could be visible going into eclipse while the silicon emission region is obscured. At the same time, the C II line is still forming in the same overall region (the corona) as the Si IV line, so these two lines might vary in the same fashion. The C IV line, on the other hand, forms in a different region (the wind), and varies differently.

The results presented here are based on observations obtained when the bright spot in IP Peg was most visible. A number of recent simulations of accretion disk structure have shown that the region where the accretion stream impacts the disk is likely to be overly dense and vertically extended (Livio, Soker, & Dgani 1986, Hirose, Osaki, & Mineshige 1991, Armitage & Livio 1996). Thus, it must be kept in mind that the flickering behavior of the lines and/or continuum is likely to be influenced by the presence of the bright spot. For example, the lack of correlation between the flickering in the UV and optical continua may be the result of the bright spot contributing more flux in one or the other of these wavelength regimes. However, the discrepancy in estimated temperatures for the bright spot in IP Peg (see §1) makes it difficult to determine which wavelength regime is more likely to be affected by the spot. Also, the fact that the IP Peg emission lines in the UV and optical are brighter at phases away from the pre-eclipse hump (Marsh 1988, Baptista et al. 1994) suggests that the bright spot may partially obscure emission line sources in the inner disk.

Doppler tomography performed on the UV emission lines in IP Peg would be most helpful in revealing the relative locations of the UV emission regions.

The observations were made with the NASA/ESA *Hubble Space Telescope*, obtained at the Space Telescope Science Institute, which is operated by the Association of Universities for Research in Astronomy, Inc., under NASA contract NAS 5-26555. The compilation of photometric data of the *Variable Star Network*, available at <http://www.kusastro.kyoto-u.ac.jp/vsnet/> and managed by D. Nogami, was extremely useful in preparing this paper. This work was supported in part by NASA grant GO-3683 to STScI and subgrants to the University of Washington (DWH and PS). DWH and PS also acknowledge NASA LTSA grant NAGW3158. AWS acknowledges NSF grant AST 9315280. ME acknowledges Hubble Fellowship grant HF-01068.01-94A.

REFERENCES

- Armitage, P. J. & Livio, M. 1996, *ApJ*, 470, 1024
- Baptista, R., Horne, K., Eracleous, M., Barwig, H., Long, K., Mantel, K.-H., Marsh, T. R., Polidan, R. S., Raymond, J. C., Robinson, E. L., Rutten, R. G. M., Shafter, A., Szkody, P., Wade, R. A., Wood, J., & Zheng, E.-H. 1994, in Shafter, A., ed., *Interacting Binary Stars*, Astronomical Society of the Pacific, San Francisco, p.259
- Eracleous, M., Horne, K., Robinson, E. L., Zhang, E.-H., Marsh, T. R., & Wood, J. H. 1994, *ApJ*, 433, 313
- Goranskij, V. P., Orlowsky, E. I., & Rahimov, V. Yu. 1985, *IBVS*, No. 2653
- Hirose, M., Osaki, Y., & Mineshige, S. 1991, *PASJ*, 43, 809
- Horne, K., & Eracleous, M. 1993, *FOS Instrument Science Report CAL/FOS-091*
- Horne, K., Marsh, T. R., Cheng, F. H., Hubeny, I., & Lanz, T. 1994, *ApJ*, 426, 294
- Kaitchuck, R. H., Schlegel, E. M., Honeycutt, R. H., Horne, K., Marsh, T. R., White, J. C. II, & Mansperger, C. S. 1994, *ApJS*, 93, 519
- Leitherer, C. 1995, *The HST Data Handbook*, v2.0, Space Telescope Science Institute, Baltimore, ch.15
- Livio, M., Soker, N., & Dgani, R. 1986, *ApJ*, 305, 267
- Marsh, T. R. 1988, *MNRAS*, 231, 1117
- Marsh, T. R. & Horne, K. 1990, *ApJ*, 349, 593
- Meyer, F. & Meyer-Hofmeister, E. 1994, *A&A*, 288, 175
- Osaki, Y. 1996, *PASP*, 108, 39
- Robinson, E. L., Wood, J. H., Bless, R. C., Clemens, J. C., Dolan, J. F., Elliot, J. L., Nelson, M. J., Percival, J. W., Taylor, M. J., van Citters, G. W., & Zhang, E. 1995, *ApJ*, 443, 295
- Shafter, A. W., Misselt, K. A., & Veal, J. M. 1993, *PASP*, 105, 853
- Szkody, P. 1987, *AJ*, 94, 1055
- Tonry, J. & Davis, M. 1979, *AJ*, 84, 1511
- Wolf, S., Mantel, K. H., Horne, K., Barwig, H., Schoembs, R., & Baernbantner, O. 1993, *A&A*, 273, 160
- Wood, J., Horne, K., Berriman, G., Wade, R., O'Donoghue, D., & Warner, B. 1986, *MNRAS*, 219, 629